Applied Catalysis B: Environmental 224 (2018) 825–835

Contents lists available at ScienceDirect

Applied Catalysis B: Environmental

journal homepage: www.elsevier.com/locate/apcatb

Research Paper

Homogeneous introduction of CeO_y into MnO_x-based catalyst for oxidation of aromatic VOCs

Jin Chen[a], Xi Chen[a,b], Xi Chen[a,b], Wenjian Xu[a], Zhen Xu[a], Hongpeng Jia[a,b,*], Jing Chen[c,d,**]

[a] CAS Center for Excellence in Regional Atmospheric Environment, and Key Laboratory of Urban Pollutant Conversion, Institute of Urban Environment, Chinese Academy of Sciences, Xiamen Fujian 361021, China
[b] University of Chinese Academy of Sciences, Beijing, 100049, China
[c] CAS Key Laboratory of Design and Assembly of Functional Nanostructures, and Fujian Provincial Key Laboratory of Nanomaterials, Fujian Institute of Research on the Structure of Matter, Chinese Academy of Sciences, Fuzhou, Fujian 350002, China
[d] Xiamen Institute of Rare-earth Materials, Haixi Institutes, Chinese Academy of Sciences, Xiamen, Fujian 361021, China

ARTICLE INFO

Keywords:
Homogeneous distribution
Catalytic oxidation
VOCs
Manganese oxide
Cerium oxide

ABSTRACT

$3MnO_x$-$1CeO_y$ (3Mn1Ce), a binary oxide with stoichiometric ratio of Mn/Ce = 3, is synthesized *via* hydrolysis driving redox. Compared to MnO_2, CeO_2, Cop-3Mn1Ce and Mixed-3Mn1Ce, the 3Mn1Ce catalyst exhibits better catalytic activity for toluene oxidation, which could be ascribed to higher concentration of active lattice oxygen, and better low-temperature reducibility, as well as homogeneous dispersion. In the test of substrate applicability, 3Mn1Ce displays good performances in the removal of benzene, *o*-xylene and chlorobenzene at moderate temperature. The application of high WHSV of 240000 mL/(g h) confirms the 3Mn1Ce catalyst still remains high efficiency to diminish toluene, giving the temperature at 280 °C for complete mineralization. A set of experiments under simulated realistic exhaust conditions demonstrate that 3Mn1Ce is a robust catalyst with high activity to oxidize mixed aromatic VOCs (BTX and chlorobenzene), satisfied endurability to high humidity (above 10–20 vol.% water) and good tolerance to severe change of reaction temperature. With characterization of XRD and TPR, the high performance is related to the homogeneous introduction of Ce resulting in higher structural stability and reversible reducibility. Moreover, the inner principle for oxidation of VOCs is revealed by comprehension of kinetic study.

1. Introduction

Volatile organic compounds (VOCs), as a large group of low boiling-point organic chemicals, are emitted from a great variety of sources, such as industrial processes, transports, house-hold activities and so on [1]. Recently, the U.S. Environmental Protection Agency has recognized over 300 chemicals as VOCs which make major contributors to air pollution [2]. Among them, the aromatic VOCs, including BTX (benzene, toluene and *o*-xylene), chlorobenzene and others, with high toxicity to human health and "carcinogenic-mutagenic-teratogenic" effect, mainly come from industrial source [3,4]. Thus, there is more increasingly strict legislation for stringent emission of industrial VOCs, causing the control technologies as a very important topic of research [5]. Nowadays, several abatement technologies (adsorption, thermal oxidation, wet scrubbing, photocatalysis, catalytic oxidation, plasma oxidation and so forth) have been used to control the release of VOCs into environment [6–8].

Among all the applied control technologies, catalytic oxidation is considered as the most efficient and economical way with harmless products (CO_2 and H_2O) and in relatively moderate conditions (at temperatures between 250 and 550 °C) for a wide range of pollutants [9–11]. Because of the dependence of the catalytic oxidation on catalysts, the search for catalytic materials with high activity, low cost and high tolerability is attracting much effort [12]. The catalysts based on noble metal, transition metal oxides and zeolite have been developed for oxidation of VOCs [12–14]. Although noble metal catalysts show remarkable activity, the high expense and low reserves of precious metal elements can limit their widely practical application; moreover, they are always subjected to deactivation from chlorine (Cl) poisoning during catalytic oxidation of chlorinated VOCs [15,16]. The high

* Corresponding author at: CAS Center for Excellence in Regional Atmospheric Environment, and Key Laboratory of Urban Pollutant Conversion, Institute of Urban Environment, Chinese Academy of Sciences, Xiamen Fujian 361021, China
** Corresponding author at: CAS Key Laboratory of Design and Assembly of Functional Nanostructures, and Fujian Provincial Key Laboratory of Nanomaterials, Fujian Institute of Research on the Structure of Matter, Chinese Academy of Sciences, Fuzhou, Fujian 350002, China; Xiamen Institute of Rare-earth Materials, Haixi Institutes, Chinese Academy of Sciences, Xiamen, Fujian 361021, China.
E-mail addresses: hpjia@iue.ac.cn (H. Jia), jing.chen@fjirsm.ac.cn (J. Chen).

https://doi.org/10.1016/j.apcatb.2017.11.036
Received 16 August 2017; Received in revised form 26 October 2017; Accepted 15 November 2017
Available online 15 November 2017
0926-3373/

activity of zeolites in removal of chlorinated VOCs is attributed to their acidic properties; however, this catalyst system would generate polychlorinated by-products, resulting in secondary pollution [15]. Compared to noble-metal catalysts and zeolite, the transition metal oxides have advantages in lower cost, better tolerability to poison, higher thermal stability and less secondary pollution, thereby attaching more and more attention [12,17,18]. However, in most researches the catalysts are studied at ideal reaction conditions where there exists only one kind of VOCs and the atmosphere is dry. In practice, the catalysts usually work at severe conditions containing complex mixture of gaseous contaminants and much moisture [19]. Therefore, it is necessary to develop a robust transition-metal catalyst with high activity to remove different kinds of VOCs and high stability to resist various interferences at realistic reaction condition.

Among the alternative transition metal oxides, manganese oxide (MnO_x) and cerium oxide (CeO_y) are common choices for catalytic oxidation of VOCs [20,21]. MnO_x not only has exhibited a comparable activity to noble-metal catalysts in the removal of gaseous pollutants, but also is a cheap and easily-obtained catalyst [22–24]. Nevertheless, the individual MnO_x is still away from arrival of satisfied catalytic performance in terms of stability and activity to some kind of VOCs, for example, the poor activity to catalytically oxidize chlorobenzene, so the introduction of the hybrid metal to form mixed metal oxides is popularly applied. Binary oxides are basic formation of mixed metal oxides. Castaño et al. reported Mn-Co mixed oxides were more active than individual manganese and cobalt oxides in catalytic combustion of toluene and propanol, which were benefited form more oxygen mobility [25]. We have also reported that Mn-Fe binary oxides were applied to catalytic oxidation of toluene and exhibited higher activity than MnO_x. It was ascribed to positive effect by the introduction of Fe element, but the Mn-Fe binary catalysts are not competent to removal of chlorinated pollutants [26]. According to the literatures, Ce-containing transition metal oxides have been considered as potential catalysts for oxidation of chlorinated VOCs, owing to their high oxygen storage capacity, abundant oxygen vacancies and strong redox property. However, the active sites of individual CeO_y catalysts are easily poisoned by Cl element, which could be overcome by the addition of secondary metals [27,28]. In fact, Mn-Ce binary oxides have been pronounced to exhibit higher catalytic efficiency and stability in oxidation of chlorinated VOCs [29,30]. As we know, these composite oxides are generally prepared by physical mixing, co-precipitation, impregnation and so on [31–34]. These methods are perhaps subjected to the limitation of element diffusion and different precipitation rates of metal precursors, resulting in heterogeneous component of as-prepared catalysts. To avoid these problems, redox co-precipitation was firstly reported by Arena et al. to realize the synthesis of Mn-Ce binary oxides with high dispersion of "molecular" level [35,36]. Subsequently, the as-prepared Mn-Ce catalysts with this synthetic method showed an improved performance in oxidation of *o*-xylene, which implied the positive effect from adequate combination of the metallic components [37]. Inspired by the above-mentioned works, we presently use the hydrolysis driving redox co-precipitation to synthesize Mn-Ce binary oxides as widely applicable catalysts for efficiently catalytic oxidation of different aromatic VOCs. It should be noted that the hydrolysis driving redox co-precipitation has been reported by us to be an effective method for synthesis of highly-dispersed Mn-Fe binay oxides [20,26].

Consequently, the Mn-Ce binary oxide was synthesized *via* our reported method to form $3MnO_x$-$1CeO_y$ (3Mn1Ce) according to the chemical stoichiometry of hydrolysis driving co-precipitation reaction. 3Mn1Ce exhibited higher activity in catalytic oxidation of toluene compared to the as-obtained catalysts with the same composition by physical mixing and classic co-precipitation. The inner relationship between catalytic behavior and structural properties was researched by combination of performance and characterization (XRD, SEM, TEM, H_2-TPR, O_2-TPD, etc.). The 3Mn1Ce catalyst still retained a remarkable activity in oxidation of different aromatic VOCs (benzene, *o*-xylene and chlorobenzene) and mixed VOCs at severe conditions of high weight hourly space velocity (WHSV), high humidity and dramatic reaction temperature change.

2. Experimental section

2.1. Chemicals and materials

All the reagents for the preparation of catalysts were A.R. grade and were used directly without further purification. Potassium permanganate ($KMnO_4$), cerium (III) nitrate hexahydrate ($Ce(NO_3)_3{\cdot}6H_2O$), manganese(II) nitrate ($Mn(NO_3)_2$, 50 wt.% aqueous solution), concentrated $NH_3{\cdot}H_2O$ solution, nitric acid (HNO_3, 65 wt.%), hydrogen peroxide (H_2O_2, 30 wt.%) and toluene were purchased from Sinopharm Chemical Reagent Co., Ltd. (Shanghai, China).

2.2. Catalyst preparation

The MnO_2 sample was synthesized by the redox reaction of $KMnO_4$ and H_2O_2 in acidic aqueous solution by our previous reported method, in which the consumption of H_2O_2 is three equivalent of stoichiometric amount [20]. On basis of this strategy, the modified procedures have been developed to prepare the Mn-Ce binary oxides by replacing acid with cerium salt. 6 g $KMnO_4$ (38.0 mmol) and 5.5 g $Ce(NO_3)_3{\cdot}6H_2O$ (12.7 mmol) were dissolved in 300 mL deionized water, and 19.45 g concentrated H_2O_2 solution (about 19.5 mmol) was diluted by 300 mL deionized water. The diluted H_2O_2 solution was added dropwise into Mn-Ce mixed solution with vigorous stirring to produce lots of precipitates. After filtering, washing and drying at 100 °C overnight, the dark-brown solids were calcined at 400 °C for 4 h in air. The obtained catalyst was denoted as $3MnO_x$-$1CeO_y$ (3Mn1Ce) corresponding to Mn/Ce stoichiometric molar ratio of 3.

The co-precipitated $3MnO_x$-$1CeO_y$ (Cop-3Mn1Ce) was prepared *via* co-precipitation method by using diluted $NH_3{\cdot}H_2O$ solution to precipitate the mixture of $Mn(NO_3)_2$ and $Ce(NO_3)_3{\cdot}6H_2O$ solution with a 3:1 molar ratio of Mn/Ce, and then calcined at 400 °C for 4 h in air. CeO_2 was synthesized by adding diluted $NH_3{\cdot}H_2O$ solution to $Ce(NO_3)_3{\cdot}6H_2O$ solution, and then calcined at 400 °C for 4 h in air. The mixed $3MnO_x$-$1CeO_y$ (Mixed-3Mn1Ce) was obtained easily by physically mixing the as-prepared MnO_2 and CeO_2 with a 3:1 molar ratio of Mn/Ce.

2.3. Catalyst characterizations

Powder X-ray diffraction (XRD) measurements were performed on PANalytical X'pert Pro instrument equipped with X-ray source of Cu-Kα at the 2θ angle range from 10° to 90°. Raman spectroscopy was carried out on LabRAM Aramis instrument equipped with a green laser of 532 nm wavelength and 18.2 mW intensity as an exciting source. S4800 scanning electronic microscopy (SEM) was taken to obtain images of samples. Transmission electronic microscopy (TEM) images of samples were given by JEM-2100F transmission electronic microscopy at both bright and dark fields. The elemental distribution of sample was investigated by using energy dispersive spectroscopy (EDS) of Oxford Instruments. The Mn, Ce and O binding energies (B.E.) of surface species were determined by Thermo Scientific ESCALAB 250 X-ray photoelectron spectroscopy instrument (XPS). H_2 temperature programed reduction (H_2-TPR) was carried out on a chemisorption instrument (Quantachrome, Chemstar) under 5% H_2/Ar gas flow of 30 mL/min at a rate of 10 °C/min. H_2 consumption was detected by TCD and was calibrated according to loading weight of samples. Notably, the procedure of repeated H_2-TPR for detecting the reversibility of reducibility at low temperature was different with the common H_2-TPR. Oxygen temperature programed desorption (O_2-TPD) was also carried out on chemisorption instrument using 20% O_2/He and pure He. The H_2-TPR, O_2-TPD and repeated H_2-TPR were described in detail in the supporting

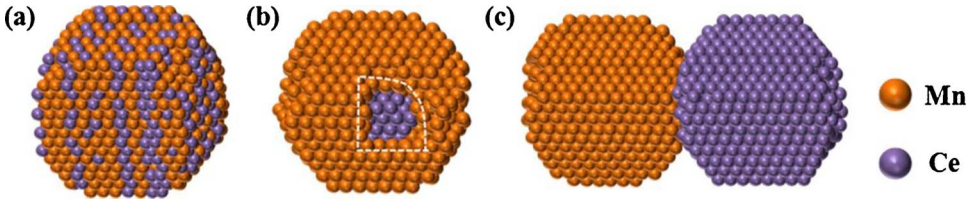

Scheme 1. The illustration of nanostructure: (a) 3Mn1Ce, (b) Cop-3Mn1Ce and (c) Mixed-3Mn1Ce.

information. The porosity of the samples was determined by N_2 static adsorption-desorption using a Quantachrome Autosorb IQ instrument. The values of specific surface areas and pore size distributions were calculated by means of the Brunauer-Emmett-Teller (BET) and Barrett-Joyner-Halenda (BJH) methods, respectively. The metal element contents of catalysts were detected using inductively coupled plasma-optical emission spectroscopy (ICP-OES). The element compositions on the surface of sample were measured by XPS. The gaseous components in the effluent gas can be identified by on-line mass spectroscopy (Tilon Company, TC-D200 M).

2.4. Catalytic test

The catalytic combustion of VOCs was carried out on the fixed bed reactor (i.d. = 6.0 mm, length = 410 mm) to evaluate catalytic performance using 66.6 mg of catalysts (40 − 60 mesh) without any pretreatment. The length of catalyst layer was 2 − 2.5 cm, and reaction temperature was measured at the bottom of reaction layer (to see the details in Fig. S1). Before catalytic test, the conditions were adjusted to avoid possibility of transfer barrier including internal and external transfer limitations. Using ignition curve to evaluate catalytic activity, the reaction temperature was elevated step-by-step and kept at target value in a certain time to wait for reaction equilibrium. For catalytic test of single VOC species, the pure air stream containing 1000 ppm of VOC passed through the catalyst layer with the total flow rate of 66.6 mL/min, giving a WHSV of 60000 mL/(g h). To investigate the influence of different WHSV, the amount of catalyst and the total flow rate were adjusted to the demands of WHSV = 120000 mL/(g h) and WHSV = 240000 mL/(g h). To investigate the effect of water vapor, 10 vol.% and 20 vol.%, were introduced by passing the feed stream through a water saturator (some water in U-type absorption glass tube) at certain temperatures. In the interrupt experiment to investigate the structural stability, the catalyst initially worked at low temperature, and then was reused at low temperature after reactivation at high temperature while the WHSV was controlled at 60000 mL/(g h). In fact, there are complex VOCs pollutants rather than simple species in industrial off-gas. Thus, to evaluate the performance in catalytic oxidation by using the mixed VOCs as the simulated industrial off-gas, the mixture of benzene, toluene, chlorobenzene and *o*-xylene was applied to generate the polluted gas containing mixed VOCs with certain concentrations (*c*(benzene) = 1400 ppm, *c*(toluene) = 500 ppm, *c*(chlorobenzene) = 300 ppm, and *c*(*o*-xylene) = 150 ppm). The composition of the outlet gas from the reactor was analyzed by the on-line gas chromatography (GC) equipped with a FID and a TCD. The conversion (X_{VOC}) and total conversion (X_{Total}) of mixed VOCs were calculated by the difference of VOCs concentration and the mineralization (Y_{CO2}) was evaluated using the changing in CO_2 concentration.

$$X_{VOC} = \frac{c(VOC)_{Outlet}}{c(VOC)_{Inlet}} \times 100\%$$

$$X_{Total} = \frac{\sum X_{VOC} \times c(VOC)}{\sum c(VOC)}$$

$$Y_{CO2} = \frac{c(CO_2)_{Outlet}}{c(CO_2)_{Complete}} \times 100\%$$

3. Results and discussion

3.1. Characterization of catalyst

As described above, the Mn-Ce binary oxides were synthesized by three strategies. Cop-3Mn1Ce and Mixed-3Mn1Ce as controlled catalysts were prepared *via* co-precipitation and physical mixing, respectively. Because the vast difference in solubility product constants (K_{sp}^{θ}) of $Ce(OH)_3$ and $Mn(OH)_2$ ($K_{sp}^{\theta}([Ce^{3+}][OH^-]^3) = 1.5 \times 10^{-20}$ and $K_{sp}^{\theta}([Mn^{2+}][OH^-]^2) = 1.9 \times 10^{-13}$) causes the easier precipitation of Ce^{3+} ions than Mn^{2+} ions during synthesis of Cop-3Mn1Ce, the preferred self-aggregation of $Ce(OH)_3$ before well-dispersion in $Mn(OH)_2$ precipitate lead to Mn-rich shell surrounding CeO_y core after calcination (Scheme 1(b)) [38]. The Mixed-3Mn1Ce catalyst has no direct interaction between MnO_2 and CeO_2 like the structure in Scheme 1(c). To overcome heterogeneous element distribution in co-precipitation and physical mixing, 3Mn1Ce was synthesized by hydrolysis driving redox co-precipitation, where a spontaneous reaction as Eq (1) consists of reduction of MnO_4^- ions (Eq (2)) and hydrolysis of Ce^{3+} salts (Eq (3)). Considering the synchronous precipitation of MnO_2 and $Ce(OH)_3$ during reaction, the as-prepared 3Mn1Ce may exist as homogeneous "solid solution" like Scheme 1(a).

$$6MnO_4^-\ (aq) + 2Ce^{3+}\ (aq) + 9H_2O_2\ (l) = 6MnO_2\ (s) + 2Ce(OH)_3\ (s) + 6H_2O\ (l) + 9O_2\ (g) \quad (1)$$

$$2MnO_4^-\ (aq) + 3H_2O_2\ (l) + 2H^+\ (aq) = 2MnO_2\ (s) + 3O_2\ (g) + 4H_2O\ (l) \quad (2)$$

$$Ce^{3+}\ (aq) + 3H_2O\ (l) \leftrightharpoons Ce(OH)_3\ (s) + 3H^+\ (aq) \quad (3)$$

Table 1
Element composition and physical properties of samples

Samples	ICP-OES		Mn/Ce molar ratio		S_{BET} (m^2/g)	D[b] (nm)	O_{Latt}/O_{Ads}
	Mn (wt.%)	Ce (wt.%)	ICP-OES	XPS[a]			
MnO_2	64.01	–	–	–	166.0	24.2	1.38
CeO_2	–	80.95	–	–	87.9	5.9	1.03
3Mn1Ce	38.96	31.43	3.16	3.01	128.4	29.7	1.67
Cop-3Mn1Ce	41.09	34.35	3.05	8.91	63.9	18.0	1.52
Mixed-3Mn1Ce	38.13	33.60	2.89	3.13	140.2	12.8	–

[a] Although the accuracy for element analysis from XPS is limited by some deviation [39,40], the results are still competent to distinguish the difference.
[b] *D* is the average pore diameter which is calculated by BJH method.

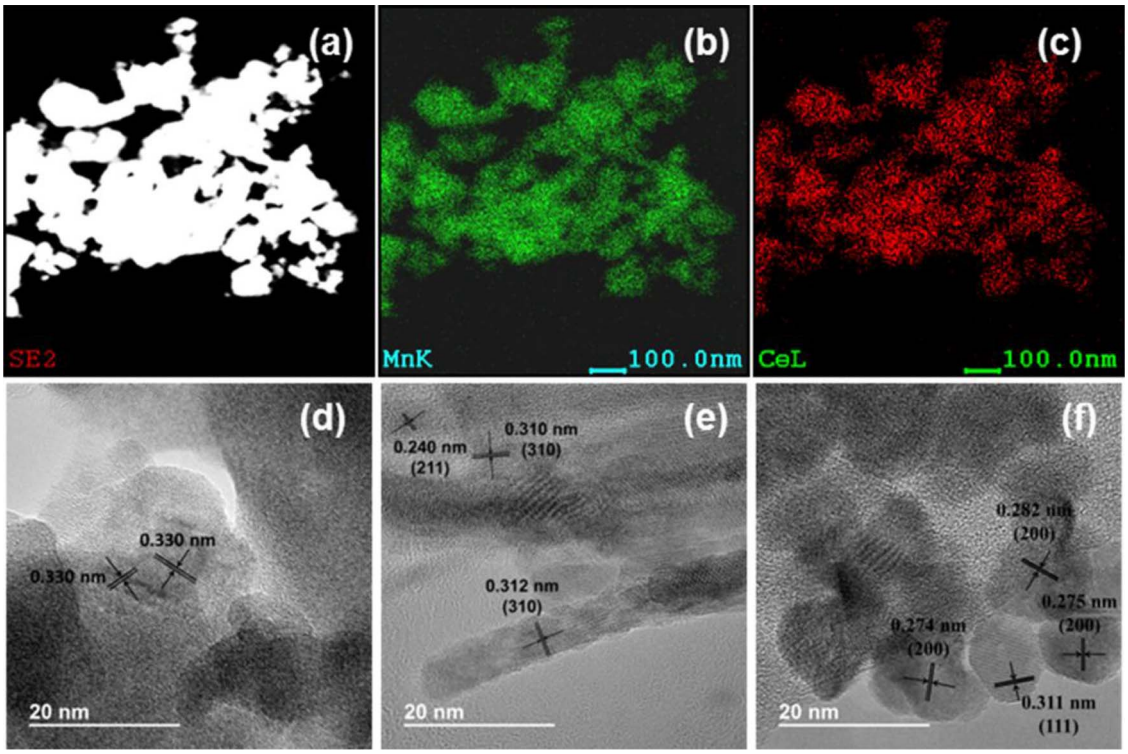

Fig. 1. (a) HAADF-STEM image, (b) Mn-element mapping, (c) Ce-element mapping of 3Mn1Ce, and HRTEM images of 3Mn1Ce (d), MnO_2 (e) and CeO_2 (f), respectively.

The element composition of samples in bulk was analyzed by ICP-OES. As listed in Table 1, the metallic element contents of MnO_2 and CeO_2 are close to nominal composition (Mn/MnO_2 = 63.2 wt.% and Ce/CeO_2 = 81.4 wt.%), and the molar ratios of Mn/Ce for Mn-Ce binary oxides are approximate to nominal ratios. With analysis of XPS spectra, the element distribution in superficial layer of binary oxides was calculated according to the area of Mn-2p and Ce-3d peaks (Fig. S2 and Table S1). As shown in Table 1, 3Mn1Ce and Mixed-3Mn1Ce exhibit the Mn/Ce XPS ratios are close to their ICP-OES results and nominal ratios. However, the Mn/Ce XPS ratio (8.91) for Cop-3Mn1Ce is much higher than that of ICP-OES result as well as the nominal ratio, which confirms the enrichment of Mn element in the superficial layer, owing to the difference in precipitation rates of Mn^{2+} and Ce^{3+} ions. To further investigate the elemental distribution of 3Mn1Ce, high-angle annular dark-field scanning transmission electron microscopy (HAADF-STEM) and EDS have also been applied. As depicted in Fig. 1(a)-(c), the overlapping of element mapping demonstrates that Mn and Ce in 3Mn1Ce are homogeneously dispersed. This phenomenon is in accordance with the results of ICP-OES and XPS analysis, which confirms our synthetic pathway is effective to form binary oxides with homogenous dispersion of Mn and secondary metal (Fe or Ce). However, Mn-rich phase deposition is obviously observed from the images of HAADF-STEM mapping for Cop-3Mn1Ce sample (Fig. S3) as an indication of agglomerates of Mn oxide, owing to the different solubility product constant of Mn and Ce ions in co-precipitation.

Generally, the differences in element composition and distribution have close relationship with structural properties. Thus, it is necessary to investigate structural features of as-prepared catalysts through a variety of characterizations. The XRD results of the obtained MnO_2, CeO_2 and binary oxides are depicted in Fig. 2. MnO_2 exhibits several weak peaks at 28.7°, 37.4°, and 56.7° (2θ), which is closer to the standard pattern of α-MnO_2 (PDF # 00-012-0706). It has been confirmed that poor crystallinity results in the absence and weakening intensity of peaks. XRD pattern for the obtained CeO_2 is indexed to the standard of typical CeO_2 (PDF # 01-081-0792). The sharp peaks corresponding to CeO_2 are only observed in XRD pattern of Mixed-3Mn1Ce. Although the characteristic peaks of CeO_2 and α-MnO_2 are seen in XRD pattern of Cop-3Mn1Ce, the slight shifts take place to the positions of these peaks especially the sharp peak at 29.0° (2θ) corresponding to CeO_2 (111) or α-MnO_2 (310) lattice plane, which indicates intense interaction between MnO_x and CeO_y. Different from the other binary oxides, the disappearance of peaks in XRD pattern of 3Mn1Ce pronounces the amorphous architecture, thus it is deduced that the introduction of Ce ions into the lattice of MnO_2 causes crystal disorder [41,42]. The more evidences are given by high resolution transmission electron microscopy (HRTEM) in Fig. 1(d)-(f). It seems quite difficult to search for sharp lattice fringes in image of 3Mn1Ce compared to those of MnO_2 and CeO_2. Moreover, the average distance of scarce lattice fringes in image of 3Mn1Ce (0.330 nm) is larger than those of MnO_2 (310) and CeO_2 (111) lattice planes. These symbols further confirm the Ce ions are introduced into the MnO_2 lattice matrix leading to non-crystallization, which encourages the occurrence of the lattice defects and the exposure of inner atoms [43–45].

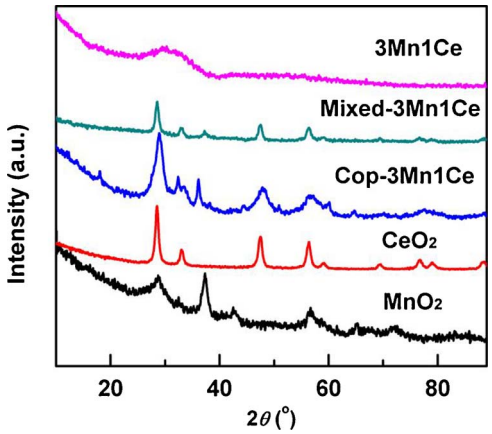

Fig. 2. XRD patterns of the samples.

N_2 absorption-desorption isotherms of MnO_2, CeO_2 and all the Mn-

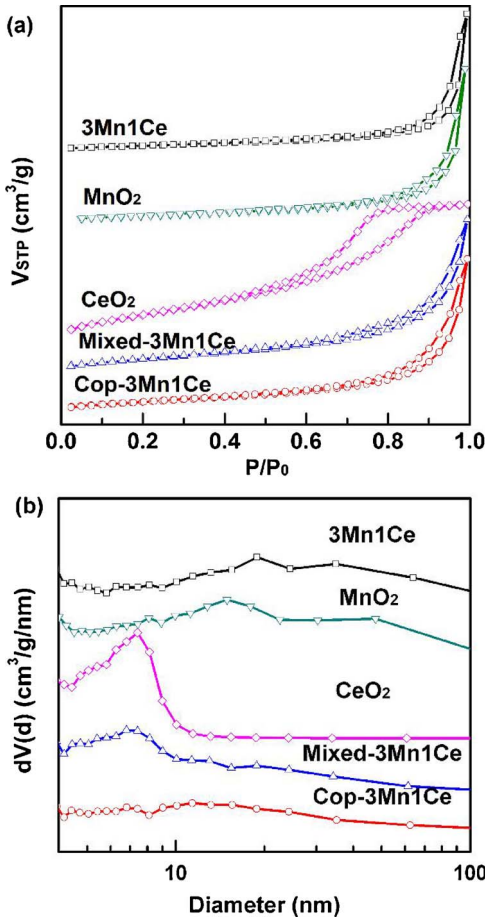

Fig. 3. (a) N_2 static absorption-desorption isotherms, and (b) the distribution of pore size.

Ce binary oxides exhibit typical features of type IV isotherms with an H3 hysteresis loop (Fig. 3(a)). According to desorption curve, the pore size distribution was calculated by means of Barrett-Joyner-Halenda (BJH) method. As shown in Fig. 3(a), all the materials possess hierarchical pore structure, where the smaller pores are inherent pores of nanoparticles and the larger ones come from stacking of nanoparticles. Among them, the larger stacking-type pores of MnO_2 and 3Mn1Ce at the range between 20 nm and 40 nm indicate the loose structures confirmed by SEM images (Fig. S4), mainly attributed to the inhibited agglomeration of small particles by great emission of O_2 during the redox reaction. For a better comparison, the relevant parameters including specific surface area (S_{BET}) and average pore diameter (D) are summarized in Table 1. The D values of MnO_2 (24.2 nm) and 3Mn1Ce (29.7 nm) are larger than those of CeO_2 (5.9 nm) and Cop-3Mn1Ce (18.0 nm). The S_{BET} values of MnO_2 (166.0 m^2/g) and 3Mn1Ce (128.4 m^2/g), prepared *via* redox reaction, are obviously higher than those of CeO_2 (87.9 m^2/g) and Cop-3Mn1Ce (63.9 m^2/g). In general, the larger pore size and higher S_{BET} are believed to be beneficial to reduce transfer resistance and improve catalytic performance. Because Mixed-3Mn1Ce was formed by physically mixing MnO_2 and CeO_2, the natures of the both oxides are mainly remained, which makes the S_{BET} and D values of Mixed-3Mn1Ce smaller due to the mutual fill.

To investigate the reducibility of 3Mn1Ce, H_2-TPR experiments were performed using MnO_2, CeO_2, and Cop-3Mn1Ce as reference samples and all the normalized results are shown in Fig. 4. The MnO_2 spectrum exhibits two obvious peaks at 294 °C and 348 °C, corresponding to the reduction of MnO_2 to Mn_2O_3 and Mn_2O_3 to Mn_3O_4 [33,42], and no reduction peak at higher temperature is observed. In TPR spectrum of CeO_2, there are three broad peaks centered at 382 °C, 510 °C and 831 °C, belonging to the easy reduction of surface Ce^{4+} species, surface reduction of capping oxygen in lattice and the reduction of the bulk of CeO_2 to Ce_2O_3 as an end-state [46,47]. Compared to MnO_2 (5870 μmol/g), the total amount of H_2 consumption of CeO_2 (1265 μmol/g) at the temperature range from 50 °C to 900 °C is much less (Table 2), as an indication of less content of reducible oxygen species. 3Mn1Ce and Cop-3Mn1Ce consume moderate amount of H_2 between MnO_2 and CeO_2. In fact, not all the oxygen takes part into the redox reaction, but the oxygen species reacting with H_2 at low temperature (below 400 °C) is related to catalytic performance which is reflected onto low-temperature reducibility, so the initial H_2 consumption rate ($r_{Initial}$) at low temperature is applied to estimate the difference of reducibility (to see the detail in SI). As shown in Fig. 4(b), the increasing order of low-temperature reducibility as follows: CeO_2 < MnO_2 < Cop-3Mn1Ce < 3Mn1Ce, implies homogeneous introduction of hybrid Ce element into MnO_2 *via* our method can enhance reducibility of catalyst at operating temperature range.

The type and mobility of oxygen species were further determined by O_2-TPD. As depicted in Fig. 4(c), all the oxides show peaks at low temperature (100 − 500 °C, *LT*) for desorption of physisorbed molecular oxygen and chemisorbed oxygen in layer on/near the surface of materials, and peaks at high temperature (500 − 900 °C, *HT*) for desorption of oxygen from the framework of materials in the bulk, respectively [48]. The catalytic reactions usually occur at the temperature less than 500 °C, the main attention is focused onto the desorption behavior of *LT* oxygen, thus the *LT* peaks are analyzed by peak–peak fitting as depicted in Fig. 4(d). In spectrum of MnO_2, there are four peaks maximized at 122 °C, 190 °C, 333 °C and 461 °C, which are corresponding to physisorbed molecular oxygen (O_{Phy}), chemisorbed oxygen on the surface (O_{Suf}), chemisorbed oxygen in lattice layer of the surface (O_{Latt}), and chemisorbed oxygen in deep lattice layer near to the surface (O'_{Latt}) [49]. The four peaks are also observed in O_2-TPD spectra of CeO_2, Cop-3Mn1Ce and 3Mn1Ce, but their locations change with the variety of samples. Considering the temperatures (150 − 400 °C) for catalytic removal of VOCs in the present work are close to the range for desorption of O_{Latt}, the performance in catalytic oxidation of VOCs is tightly related to the O_{Latt}. With comparison of the desorption temperatures, the mobility of O_{Latt} can be ranked as order: CeO_2 (235 °C) > 3Mn1Ce (255 °C) > Cop-3Mn1Ce (286 °C) > MnO_2 (333 °C), which is in line with the chang of apparent activation energy for catalytic oxidation of toluene. The amount of oxygen absorption in O_2-TPD experiment is quantified in Table 2. Although the total amount of desorbed oxygen of MnO_2 (3040 μmol/g) is the most among the catalysts, the portion of O_{Latt} in MnO_2 is only 6.2% (188 μmol/g) and is obviously less than that in CeO_2 (15.7%). The introduction of Ce into MnO_2 to form binary oxides could improve the content of O_{Latt}, and the promotion effect of our synthetic method is exhibited more strongly, so the 3Mn1Ce catalyst has more portion of O_{Latt} than Cop-3Mn1Ce.

XPS was used to further determine the type and content of oxygen species on/in superficial layer of as-prepared catalysts. As depicted in Fig. 5, the binary oxides and MnO_2 possess two peaks at 531.7 – 531.3 eV and 529.8–529.6 eV corresponding to adsorbed oxygen (O_{Ads}) and surface lattice oxygen (O_{Latt}). The peaks of CeO_2 at 533.3 eV and 531.3 eV is associated with adsorbed water molecule and adsorbed oxygen (O_{Ads}), and the peak at 529.3 eV is assigned to O_{Latt} [30,47,50]. It is noted that the more anionic property of oxide ions in CeO_2 than those in MnO_2 gives rise to lower binding energy (B.E.) of O-1s. The "Mn ⟵ O" electron-transfer processes enable formation of electrophilic oxygen in binary oxides which is confirmed by moderate B.E. for O–1 s of Cop-3Mn1Ce (531.3 and 529.7 eV) and 3Mn1Ce (531.3 and 529.6 eV) [29,30,51]. Moreover, the O_{Latt}/O_{Ads} atomic ratios over these fresh samples were estimated by the quantitative analysis and summarized in Table 1. Among them, 3Mn1Ce exhibits the higher values of O_{Latt}/O_{Ads} ratio than those of MnO_2, CeO_2 and Cop-3Mn1Ce, which is thought to be beneficial to Mars-van-Krevelen mechanism for VOCs oxidation [17,52].

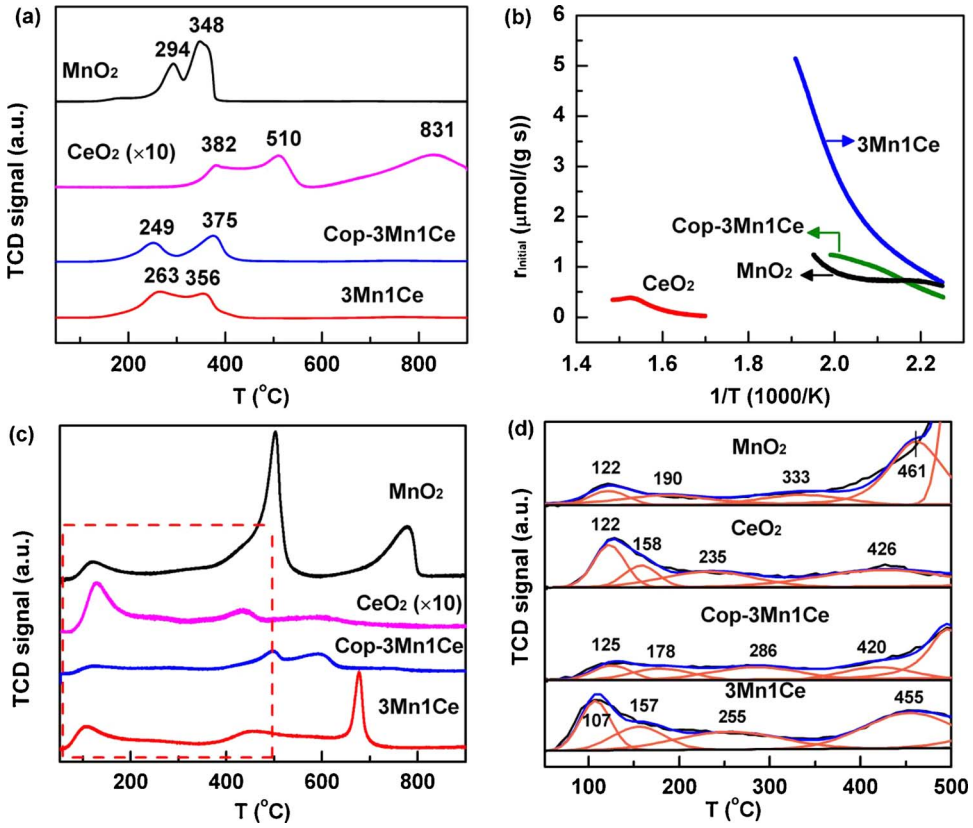

Fig. 4. (a) H_2-TPR profiles and (b) initial H_2 consumption rate ($r_{initial}$) at low temperature, (c) O_2-TPD at the temperature range of 50 − 900 °C and (d) the peak–peak fitting O_2-TPD profiles at the temperature range of 50 − 500 °C.

Table 2
Quantitative results of H_2-TPR and O_2-TPD.

Samples	Amount of H_2 in H_2-TPR (μmol/g, 50–900 °C)	Amount of desorbed O_2 in O_2-TPD (μmol/g)					O_{Latt}/O_{Total} in O_2–TPD (%)
		Total amount (50–900 °C)	O_{Phy}	O_{Suf}	O_{Latt}	O'_{Latt}	
MnO_2	5870	3040	115	274	188	884	6.2
CeO_2	1265	477	69	38	75	121	15.7
3Mn1Ce	5631	1696	196	157	242	415	14.3
Cop-3Mn1Ce	3840	1367	63	80	134	107	9.8

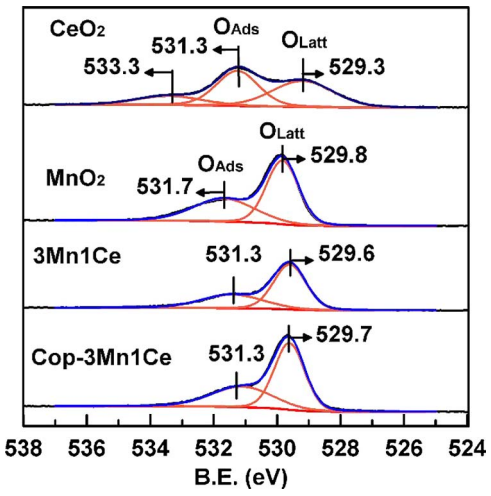

Fig. 5. O–1 s XPS profiles corresponding to the as-prepared mono-metal oxides and binary oxides with different synthetic methods.

3.2. Catalytic performance

The results of the catalytic evaluation in combustion of aromatic VOCs including toluene, benzene, chlorobenzene and *o*-xylene, are shown in Fig. 6, where the catalytic performance was tested under the conditions of VOCs concentration = 1000 ppm, WHSV = 60000 mL/(g h), and pure air as the feed gas. As listed in Table 3, the $T_{50\%}$ as required temperatures for 50% VOCs conversion and 50% CO_2 yield are used to conveniently evaluate catalytic activity at low temperature, meanwhile, the high-temperature catalytic activity is evaluated on basis of temperatures for 90% VOCs conversion and 90% CO_2 yield. According to the values of $T_{50\%}$ for toluene conversion and mineralization, the 3Mn1Ce (226 °C, 231 °C) exhibits the better performance in catalytic oxidation of toluene than the other catalysts, CeO_2 (232 °C, 235 °C) is the second active catalyst, and all the binary oxides (3Mn1Ce, Cop-3Mn1Ce and Mixed-3Mn1Ce) show higher activity than MnO_2 (252 °C, 255 °C). From seeing the changing of $T_{90\%}$ for toluene conversion and mineralization, the high-temperature catalytic activities are ranked as follows: 3Mn1Ce (239 °C, 247 °C) > Mixed-3Mn1Ce (256 °C, 260 °C) ≥ Cop-3Mn1Ce (256 °C, 268 °C) > MnO_2 (267 °C, 273 °C) > CeO_2 (280 °C, 285 °C). Generally, it is considered that there are several main factors determining the catalytic activity of metal oxides such as structures, morphologies, and redox properties [53], derived from the nature of metals as well as improved by the optimized preparation method. According to the previous discussion about structural characterizations, the succession of hydrolysis driving redox co-precipitation in homogeneously mixing two elements gives 3Mn1Ce catalyst a preferable low-temperature reducibility, proper natures of oxygen desorption and the higher content of O_{Latt}, which are beneficial to VOCs combustion. If only on basis of $T_{50\%}$, the second active catalyst is CeO_2 ascribed to the high mobility of O_{Latt} according to O_2-TPD characterization, but the complete oxidation of toluene into CO_2 over CeO_2 demands severe condition of the reaction temperature as high as 320 °C, due to the low content of O_{Latt}. This phenomenon had also been

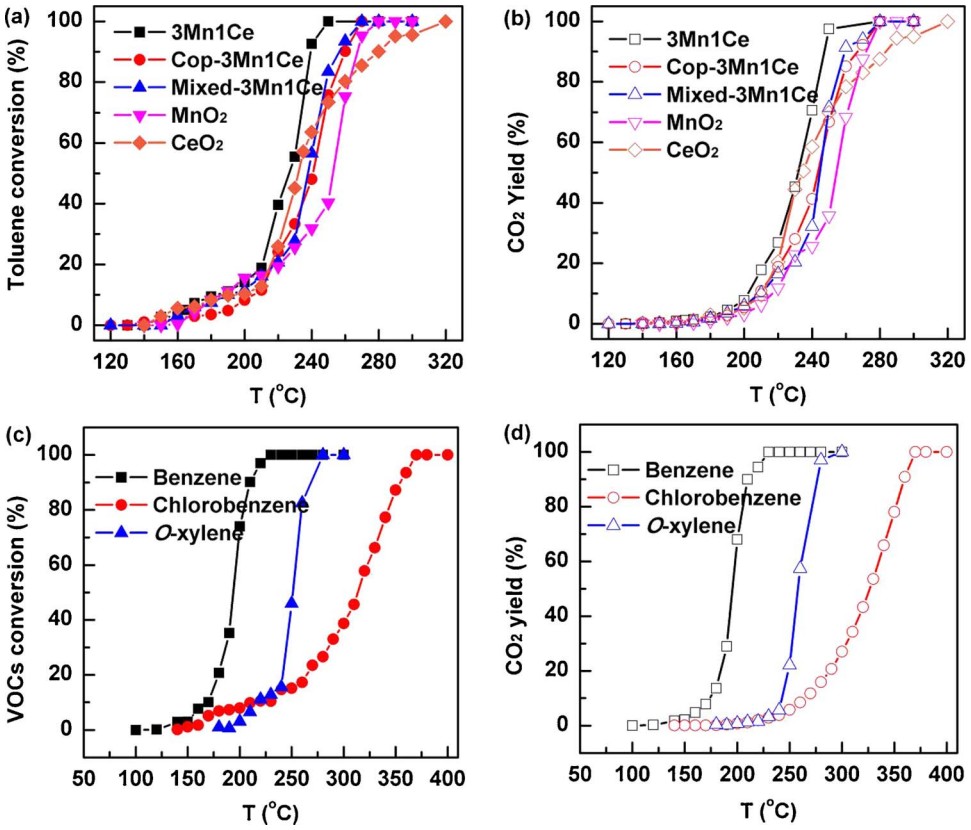

Fig. 6. The activity test in catalytic oxidation of VOCs at WHSV of 60000 mL/(g h): (a) toluene conversion over all the catalysts, (b) CO_2 yield from toluene oxidation over all the catalysts, (c) conversion of different aromatic VOCs over 3Mn1Ce, (d) CO_2 yield from catalytic combustion of various aromatic VOCs over 3Mn1Ce.

found by Delimaris et al. [42]. It is noted the relatively higher temperature is required for CO_2 yield than toluene conversion, owing to the formation of several intermediates. With the analysis of composition in the effluent gas by using on-line MS, benzoic acid, benzaldehyde and maleic acid were recognized from the partial oxidation of toluene, and a bit of unidentified components with high molecular mass were also found as shown in Fig. S5. The intermediates are easily covered on the surface of catalyst to form carbon deposit, thus leading to the relatively higher temperature for the deep oxidation of toluene.

In dynamic study on the catalytic behavior, the E_{App} values of each catalyst for toluene conversion and mineralization were respectively calculated according to the slope values for linear-fitting Arrhenius plots in Fig. S6. Notably, the conversion and CO_2 yield are monitored below 20% for dynamic calculation, and all the results of E_{App} are summarized in Table 3. According to the E_{App} values, the activities in catalytic conversion of toluene decrease as follows: CeO_2 (49.7 kJ/mol) > 3Mn1Ce (52.4 kJ/mol) > Mixed-3Mn1Ce (54.9 kJ/mol) > Cop-3Mn1Ce (64.8 kJ/mol) > MnO_2 (73.6 kJ/mol), and the capabilities for catalytic mineralization of toluene into CO_2 decrease as the order: 3Mn1Ce (88.1 kJ/mol) > CeO_2 (90.9 kJ/mol) > Mixed-3Mn1Ce (101.4 kJ/mol) ≈ Cop-3Mn1Ce (100.6 kJ/mol) > MnO_2 (113.7 kJ/mol). The higher energy barrier for CO_2 formation than that for toluene conversion is in line with the activity test where the CO_2 yield requires higher temperature than conversion of toluene. The change in E_{App} values could reflect variation tendency of low-temperature catalytic activity, which is ranked on basis of $T_{50\%}$ for toluene conversion and CO_2 yield.

To investigate the adaptability of 3Mn1Ce to various VOCs, benzene, *o*-xylene and chlorobenzene were chosen as candidates to carry out the catalytic tests. As shown in Fig. 6(c) and 6(d), the performance of 3Mn1Ce in VOCs conversion and CO_2 formation depends on the kind of VOCs. According to $T_{50\%}$ for 50% conversion and CO_2 yield (in Table 3), the differences in oxidation of VOCs can be ranked as follows: chlorobenzene (314 °C, 327 °C) > *o*-xylene (251 °C, 258 °C) > toluene (226 °C, 231 °C) > benzene (194 °C, 196 °C), which is also in line with the order according to $T_{90\%}$. According to a set of experimental data

Table 3
Catalytic performances of various catalysts in oxidation of aromatic VOCs

Catalyst	Substrate	Temperature (°C)				E_{App} (kJ/mol)	
		Conversion		CO_2 yield		Conversion	CO_2 yield
		$T_{50\%}$	$T_{90\%}$	$T_{50\%}$	$T_{90\%}$		
MnO_2	Toluene	252	267	255	273	73.6	113.7
CeO_2	Toluene	232	280	235	285	49.7	90.9
Mixed-3Mn1Ce	Toluene	238	256	244	260	54.9	101.4
Cop-3Mn1Ce	Toluene	240	256	243	268	64.8	100.6
3Mn1Ce	Toluene	226	239	231	247	52.4	88.1
3Mn1Ce	*O*-xylene	251	268	258	276	59.0	103.1
3Mn1Ce	Benzene	194	210	196	210	66.5	64.0
3Mn1Ce	Chlorobenzene	314	355	327	359	147.2 (140–180 °C) 25.8 (190–260 °C)	86.5

and related analysis using Arrhenius function (Fig. S7), the E_{App} values for conversion and CO_2 yield of each VOC pollutant were calculated and all the result are listed in Table 3. In fact, catalytic oxidation of VOCs is a multiple-step reaction where the conversion is just a beginning and the CO_2 formation is the end, so the values of E_{App} for conversion and CO_2 yield are corresponding to energy barriers for activation and deep oxidation of VOCs. On the basis of the dissociation energies of C − H (110 kcal/mol on phenyl group and 75 kcal/mol on methyl group) and C − Cl bonds (96 kcal/mol on phenyl group) [54–56], during catalytic oxidation reaction the activated sites are pointed out to be C − Cl bond of chlorobenzene, C − H bond on phenyl group of benzene, and C − H bond on methyl group of toluene and *o*-xylene, respectively. Because of the steric hindrance resulted from double methyl groups, the activation of *o*-xylene has more difficulty than toluene [57]; meanwhile, the Cl element of chlorobenzene poisoning catalyst leads to a higher energy barrier for molecular activation [21,29,30,46]. Therefore, these comprehensive effects result in the change of E_{App} energy for VOCs conversion as this order: chlorobenzene (147.2 kJ/mol, 140–180 °C) > benzene (66.5 kJ/mol) > *o*-xylene (59.0 kJ/mol) > toluene (52.4 kJ/mol). The poisoning effect of Cl element is overcome by elevating reaction temperature causing the reduced E_{App} (25.8 kJ/mol, 190–260 °C) for conversion of chlorobenzene. The further oxidation of phenyl/methyl groups on activated VOCs molecule into CO_2 is mainly affected by Cl poisoning effect and steric hindrance, so the E_{App} values for CO_2 formation change as the order: *o*-xylene (103.1 kJ/mol) > toluene (88.1 kJ/mol) > chlorobenzene (86.5 kJ/mol) > benzene (64.0 kJ/mol). Interestingly, although 5Mn1Fe as an optimal catalyst in our previous work exhibited the better performance than 3Mn1Ce in the removal of toluene at the same condition, the temperature for complete oxidation of chlorobenzene over 5Mn1Fe was above 540 °C which is much higher than that over 3Mn1Ce, as depicted in Fig. S8.

In order to get a deep insight into the kinetic principle for catalytic oxidation of VOCs, all the plots of apparent prefactors ($\ln A_{App}$) in Arrhenius function versus E_{App} are presented in Fig. 7. It can be observed that the data fit into the Cremer-Constable relation: $\ln A_{App} = aE_{App} + b$, namely, a compensation effect is present. The slope (a) values of the straight lines calculated by linear regression are 0.270 mol/kJ and 0.210 mol/kJ corresponding to VOCs conversion and CO_2 yield, respectively. It should be noted the data about mineralization of chlorobenzene marked by red cycle is neglected for linearity. According to the elegant analysis of Lyngaard et al., the slope of the Constable plot should be equal to 1/RT, where T is an average temperature for reaction rate measurements; moreover, the compensation effect is observed for reactions showing nonlinearity in Arrhenius plot which is caused by differences in binding energies and activation enthalpies [42,58]. Since these contributions are likely to vary, they pronounced a compensation effect should be quite general, which means the experimentally determined slope (a) in Constable plot is close to 1/RT and independent of reaction mechanism and kinetics. In this work, the kinetic measurements of VOCs conversion were carried out in the temperature range of 100–260 °C (373–533 K), so by assuming the average temperature of 180 °C (453 K) the value of 1/RT is calculated to be 0.265 mol/kJ that is close to experimental value (0.270 mol/kJ). Given the temperature range of 100–240 °C (373–513 K) for kinetic study of CO_2 formation, the predicted value of 1/RT is 0.272 mol/kJ that is rather different from the truth (0.210 mol/kJ). Therefore, the Cremer-Constable relation is applicable for kinetic process of VOCs activation, but it does not work on the kinetics of VOCs mineralization into CO_2. This finding is easy to understand, since the activation of VOCs is just related to the interaction between catalyst and VOCs molecule, but the activation of gaseous oxygen as well as the transformation of intermediates should be also taken into account for kinetics of CO_2 formation.

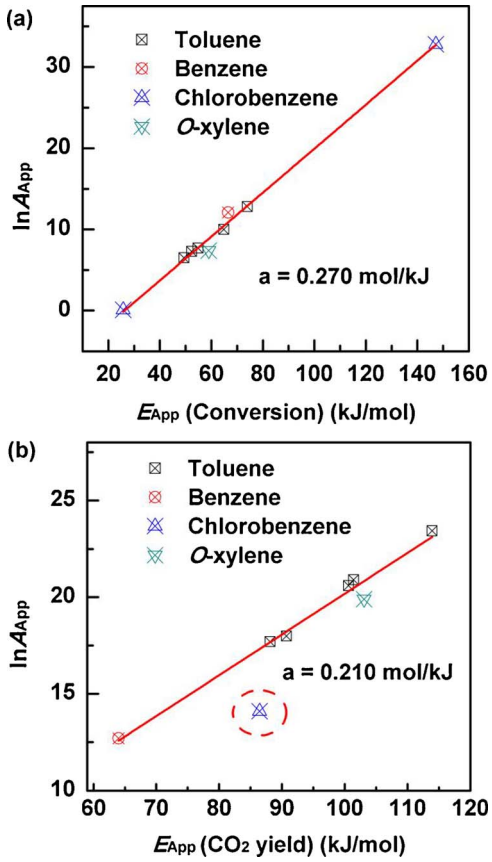

Fig. 7. Constable plot of apparent prefactors ($\ln A_{App}$) as a function of apparent activation energies (E_{App}) for oxidation of toluene over all catalysts, and benzene, chlorobenzene and *o*-xylene with respect to (a) conversion, and (b) CO_2 yield.

3.3. Tests of catalytic stability

Further, the influence of WHSV on the catalytic activity of the 3Mn1Ce catalyst has been investigated, as shown in Fig. 8. Obviously, the catalytic activity of the 3Mn1Ce catalyst is affected by the WHSV values. With the WHSV increasing from 60000 to 240000 mL/(g h), the curves of toluene conversion and CO_2 yield versus reaction temperature shift to higher temperature range. However, the complete decomposition of toluene into CO_2 was achieved by 3Mn1Ce at the temperature below 300 °C even when WHSV was raised to 240000 mL/(g h). Considering the possibility of a great deal of water vapor at real exhaust condition, the effect of humidity onto catalytic performance of 3Mn1Ce was investigated at the WHSV of 240000 mL/(g h) in the feed streams containing 10 vol.% and 20 vol.% water. As shown in Fig. 9, 3Mn1Ce achieved the complete conversion of toluene and CO_2 yield of above 95% in dry stream at 280 °C. When 10 vol.% and 20 vol.% of water vapor were introduced, the complete conversion was remained, but the CO_2 yield was reduced from 95% to 85%. It is known that the oxidation of toluene consumes oxygen and releases H_2O and CO_2, and the reaction follows a series of consequent steps (toluene → benzaldehyde → benzoic acid → maleic acid) [26]. In these steps, the conversion of toluene into benzaldehyde and benzoic acid consumes less oxygen and emits fewer amounts of CO_2 and H_2O in comparison to the further deep mineralization of benzoic acid and maleic acid into CO_2. From viewpoint of the reaction balance, the introduction of water is unfavorable for the reactions. Meanwhile, the decreasing in oxygen concentration by introducing water is negative to oxygen-consumption steps especially to the oxidation of benzoic acid and maleic acid which need more oxygen. Therefore, the introduction of water has obvious influence on the CO_2 yield than the conversion of toluene. The catalytic performance of 3Mn1Ce could be remained with a slight fluctuation at retention time

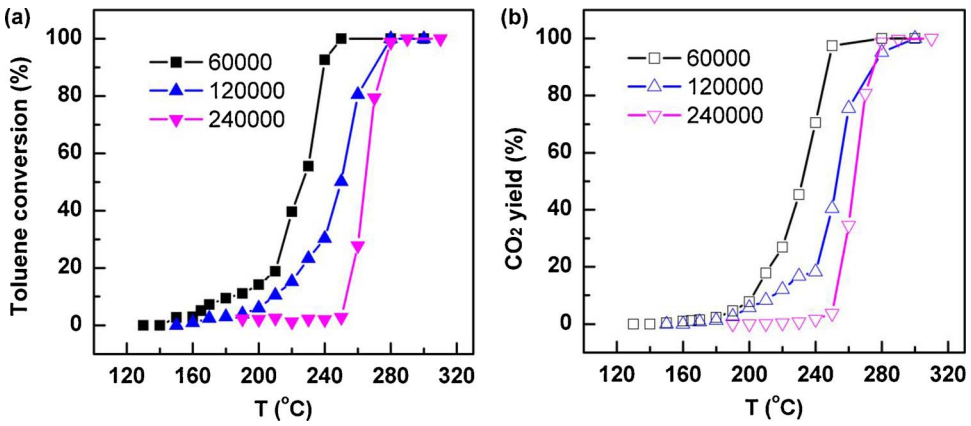

Fig. 8. Effect of WHSV onto the catalytic activity of the 3Mn1Ce catalyst, (a) toluene conversion and (b) CO_2 yield.

under humidity of 10 vol.%–20 vol.%. After humidity test, the high activity came back by flowing dry feed stream, which means a high catalytic endurability of 3Mn1Ce to humidity. However, the catalytic activity of 3Mn1Ce was decreased gradually with the prolonging reaction time under the conditions of 260 °C, 10 vol.% water and WHSV = 240000 mL/(g h) (Fig. S9), ascribing to the accumulation of intermediates on catalyst at low temperature.

Considering the real condition containing complex VOCs, the investigation on oxidation of mixed VOCs over 3Mn1Ce was carried out. The concentration of benzene, toluene, *o*-xylene and chlorobenzene in feed gas was 1400 ppm, 500 ppm, 150 ppm and 300 ppm, thereby the total concentration was 2350 ppm. As shown in Fig. 10, the activity of 3Mn1Ce decreases with prolonging retention time at 280 °C, possibly owing to poisoning effect of chlorobenzene. When the temperature is raised to 320 °C, toluene and *o*-xylene are complete eliminated, the conversion of benzene and chlorobenzene are about 50% and 45%, as a result, the total conversion and CO_2 yield are about 65% and 50%, respectively. When the temperature increases to 360 °C, the conversion and mineralization are further improved, thus the total conversion and CO_2 yield increase to around 85% and 80%, respectively. With temperature increasing to 380 °C, almost all VOCs are oxidized. When the temperature increases to 400 °C, the mixed VOCs are completely mineralized into CO_2. Then, the introduced water vapor of 10 vol.% leads to CO_2 yield declining at 380 °C, but the major portion of VOCs have been removed. These results demonstrate the 3Mn1Ce is a robust catalyst for efficient removal of VOCs at realistic reaction.

The continuous test was performed to evaluate catalytic stability of 3Mn1Ce using MnO_2 and CeO_2 as reference. Because no toluene gas pass through the catalyst layer in the progress of increasing temperature, all the fresh catalysts exhibited higher primary activities at targeted temperature than those previously presented in temperature-rising curve for activity test. As depicted in Fig. 11, when the 3Mn1Ce catalyst was exposed in stream of 1000 ppm toluene at 230 °C, the activity decreased initially which was ascribed to fast accumulation of intermediates on the surface of fresh catalyst, but then the conversion and CO_2 yield remained about 75%. During the temperature increasing to about 240 °C with heating rate of 10 °C/min, the detected temperature on catalyst layer dramatically reached to above 340 °C and then quickly came back to the control, and was continuously raised to 300 °C for reactivation (not presented here). After reactivation at 300 °C, the conversion of toluene was 100% and CO_2 yield was kept at about 80% within 720 min; finally, the increasing of temperature to 240 °C caused the complete mineralization of toluene into CO_2. After reactivation at high temperature, the gently promoted catalytic activity was also observed by Yang et al. owing to the structural change [59], which will be discussed latter. During the reaction temperature changing, the severe increasing of temperature is ascribed to sudden combustion of accumulated by-products (including maleic acid, benzoic acid, benzaldehyde, etc. which have ever been recognized [26]) on catalyst at a certain temperature. In fact, the same phenomenon of severe change in temperature during handling reaction condition also happens to MnO_2 and CeO_2. However, the activity of MnO_2 was unrecoverable after reactivation, thus the conversion and CO_2 yield were less than 80% even at the temperature of 300 °C (Fig. S10(a)). Compared to MnO_2, CeO_2 exhibited the thermal stability as high as to 3Mn1Ce, so its activity was retained during temperature changing (Fig. S10(b)).

Because volcano-shaped temperature change has influence onto the catalytic performance, it is necessary to distinguish the difference occurring in the structural natures of catalysts. The catalysts worked at the low temperature of 180 °C within 12 h in the stream of 1000 ppm toluene, which are donated as 180-MnO_2 and 180-3Mn1Ce; then the temperature was elevated from 180 °C to 240 °C, and the catalysts through the two-step treatment are named as 240-180-MnO_2 and 240-

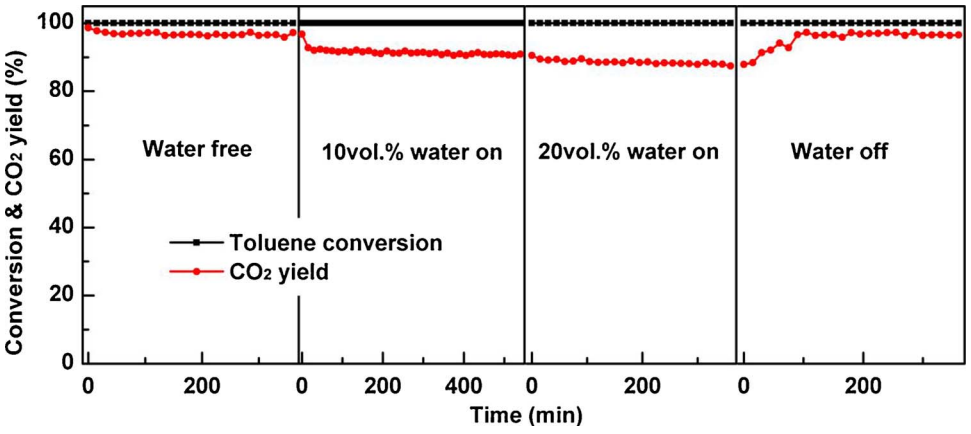

Fig. 9. The effect of humidity onto the performance of 3Mn1Ce at 280 °C in catalytic oxidation of toluene with WHSV of as high as to 240000 mL/(g h) and concentration = 1000 ppm.

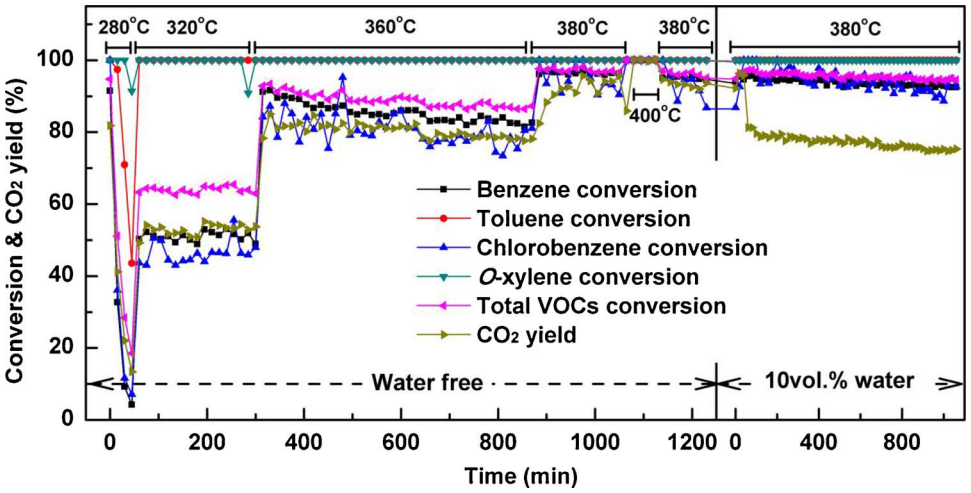

Fig. 10. The catalytic performance of 3Mn1Ce in oxidation of mixed VOCs at conditions of WHSV as high as 240000 mL/(g h) and the concentration of benzene, toluene, chlorobenzene and *o*-xylene being 1400 ppm, 500 ppm, 300 ppm and 150 ppm, respectively.

180-3Mn1Ce. From seeing Fig. 12, the intensity of peaks in XRD patterns of 180-MnO_2 and 180-3Mn1Ce seems lower than those of the fresh ones, ascribed to the accumulation of by-products in framework of catalysts. The sharp peaks of 240-180-MnO_2 imply a great deal of heat from combustion of by-products to lead to the structure sintering. The slight sharpness of peaks also takes place to 240-180-3Mn1Ce compared to 240-180-MnO_2, which indicates the better structural stability of 3Mn1Ce than MnO_2. Several inevitable changes of catalyst are caused by unpredicted factors to lead to some differences in catalytic performance [60]. As mentioned above, the long-time operation at low temperature and rapid elevation of temperature have an obvious influence onto the catalyst structure (Fig. 12). Whether the structural change is recoverable is researched by repeating temperature-programed reduction to investigate reversibility of catalyst reducibility at defined temperature range. As shown in Fig. S11, there are obvious differences in reduction curves of the first and second times for all the samples except for CeO_2. For better comparison, the intensity ratio of reduction TCD signals between the second and first times is applied. As depicted in Fig. 13, the reversibility of low-temperature reducibility is reflected onto the distance where the obtained ratio is away from the dotted line for ideal reversibility (constant ratio = 1). The intensity ratio of CeO_2 near to the ideal line indicates a high reversibility, but a great difference occurs to MnO_2 after pre-reduction implying a low reversibility. The introduction of Ce into MnO_2 by chemical method to form 3Mn1Ce and Cop-3Mn1Ce enhances the reversibility of reducibility. Among them, 3Mn1Ce exhibits a more stable reversibility than Cop-3Mn1Ce especially at the temperature above 200 °C. In our opinion, the advantages of CeO_y (including high special oxygen-storage, oxygen-removal capacity and the fast oxygen vacancy transfer ability [48,61,62]) are enlarged by highly mixing Mn and Ce *via* our method,

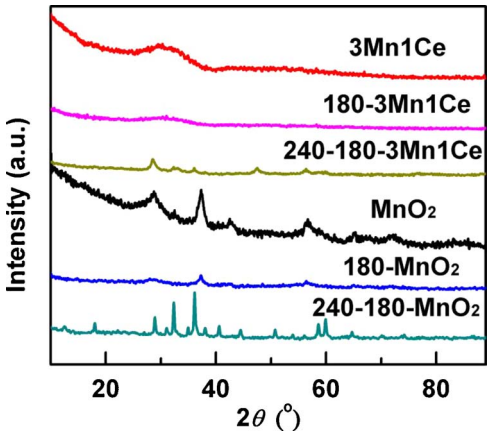

Fig. 12. XRD characterization for investigating the influence of reaction temperature onto structure of MnO_2 and 3Mn1Ce.

so 3Mn1Ce is able to perform high stability in efficiently catalytic oxidation of VOCs at severe environmental condition.

4. Conclusions

The homogenously-dispersed 3Mn1Ce is successfully prepared by hydrolysis driving redox co-precipitation method. Compared to monometal oxides (MnO_2 and CeO_2) and Mn-Ce binary oxides prepared with other methods, the improvement in physicochemical properties such as metals distributions, surface areas, structures, morphologies and reducibility of 3Mn1Ce results in the better performance in catalytic

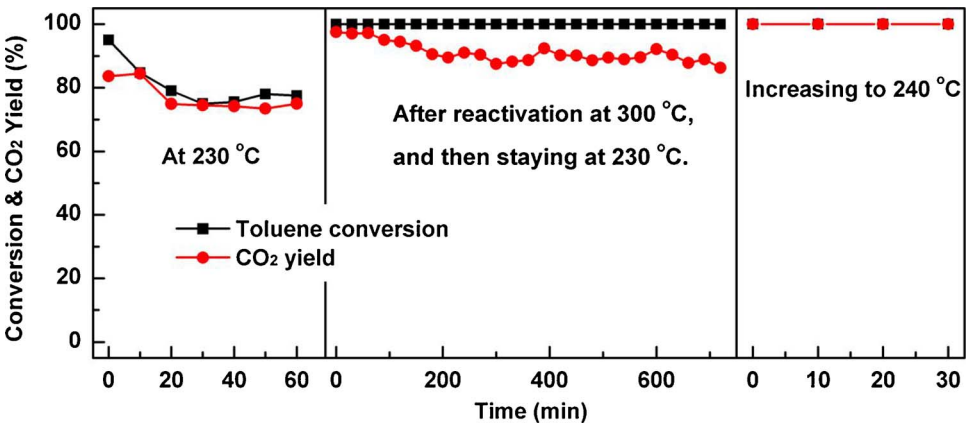

Fig. 11. Continuous test of catalytic stability of 3Mn1Ce in oxidation of toluene (1000 ppm) with WHSV of 60000 mL/(g h).

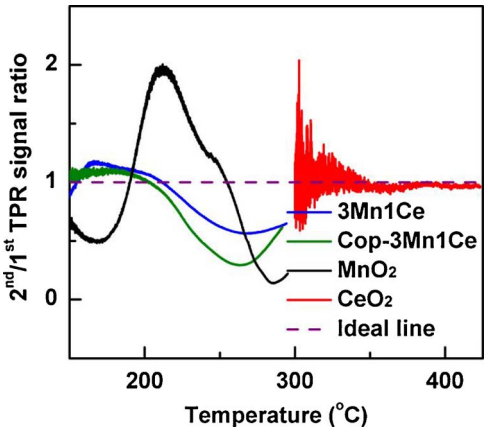

Fig. 13. The intensity ratio of TCD signals between the second and the first programed temperature in H_2-TPR.

oxidation of VOCs such as BTX (toluene, benzene, *o*-xylene) and chlorobenzene. As a result, the required temperatures for diminishing half portion of BTX and chlorobenzene are lower than 250 °C and 314 °C over 3Mn1Ce, respectively, at the conditions of concentration = 1000 ppm and WHSV = 60000 mL/(g h). The application of high WHSV of 240000 mL/(g h) confirms the high efficiency of 3Mn1Ce catalyst, giving the temperature at 280 °C for complete mineralization of toluene. A set of experiments under simulated realistic exhaust conditions demonstrate that 3Mn1Ce is a robust catalyst with high activity to oxidize aromatic VOCs mixture, satisfied endurability to high humidity (10 − 20 vol.% water) and good tolerance to severe change of reaction temperature. With systemic kinetics studies about different kinds of VOCs oxidation over various catalysts, the principles for activation of VOCs and CO_2 formation are revealed to be different.

Acknowledgements

This work was supported by Nature Science Foundation of Fujian Province of China [No. 2016J01079, No. 2016J05049]; "Cooperation of Industry-University-Institute and Scientific and Technological Cooperation" of Xiamen [3502Z20172025]; the "One Hundred Talent Project" from Chinese Academy of Sciences; the "Xiamen High-level Overseas Innovation Talent" from Xiamen; the "Key Research Program of Frontier Sciences" from Chinese Academy of Sciences [No. QYZDB-SSW-DQC022]; National Natural Science Foundation of China [No. 21501175].

Appendix A. Supplementary data

Supplementary data associated with this article can be found, in the online version, at http://dx.doi.org/10.1016/j.apcatb.2017.11.036.

References

[1] L.F. Liotta, Appl. Catal. B 100 (2010) 403–412.
[2] M. Piumetti, D. Fino, N. Russo, Appl. Catal. B 163 (2015) 277–287.
[3] M. Hakim, Y.Y. Broza, O. Barash, N. Peled, M. Phillips, A. Amann, H. Haick, Chem. Rev. 112 (2012) 5949–5966.
[4] S.H. Taylor, Top. Catal. 52 (2009) 457–457.
[5] R. Atkinson, Atmos. Environ. 34 (2000) 2063–2101.
[6] J. Zhao, X.D. Yang, Build. Environ. 38 (2003) 645–654.
[7] J.J. Spivey, Ind. Eng. Chem. Res. 26 (1987) 2165–2180.
[8] H.L. Chen, H.M. Lee, S.H. Chen, M.B. Chang, S.J. Yu, S.N. Li, Environ. Sci. Technol. 43 (2009) 2216–2227.
[9] K. Everaert, J. Baeyens, J. Hazard. Mater. 109 (2004) 113–139.
[10] G.L. Zhou, H. Lan, T.T. Gao, H.M. Xie, J. Chem. Eng. 246 (2014) 53–63.
[11] R.S. Peng, X.B. Sun, S.J. Li, L.M. Chen, M.L. Fu, J.L. Wu, D.Q. Ye, J. Chem. Eng. 306 (2016) 1234–1246.
[12] W.B. Li, J.X. Wang, H. Gong, Catal. Today 148 (2009) 81–87.
[13] L.L. Zhang, S.Y. Liu, G.Y. Wang, J.X. Zhang, React. Kinet. Mech. Catal. 112 (2014) 249–265.
[14] B. Puértolas, A. Smith, I. Vázquez, A. Dejoz, A. Moragues, T. Garcia, B. Solsona, J. Chem Eng 229 (2013) 547–558.
[15] J.W. Kan, L. Deng, B. Li, Q. Huang, S.M. Zhu, S.B. Shen, Y.W. Chen, App. Catal. A 530 (2017) 21–29.
[16] Y.B. Li, C.B. Zhang, J.Z. Ma, M. Chen, H. Deng, H. He, Appl. Catal. B 217 (2017) 560–569.
[17] Z. Ren, Z.L. Wu, W.Q. Song, W. Xiao, Y.B. Guo, J. Ding, S.L. Suib, P.X. Gao, Appl. Catal. B 180 (2016) 150–160.
[18] M. Romero-Sáez, D. Divakar, A. Aranzabal, J.R. González-Velasco, J.A. González-Marcos, Appl. Catal. B 180 (2016) 210–218.
[19] V. Blasin Aubé, J. Belkouch, L. Monceaux, Appl. Catal. B 43 (2003) 175–186.
[20] J. Chen, X. Chen, Z. Xu, W.J. Xu, J.J. Li, H.P. Jia, J. Chen, ChemistrySelect 1 (2016) 4052–4056.
[21] C. He, B.T. Xu, J.W. Shi, N.L. Qiao, Z.P. Hao, J.L. Zhao, Fuel Process. Technol. 130 (2015) 179–187.
[22] K. Ramesh, L.W. Chen, F.X. Chen, Y. Liu, Z. Wang, Y.F. Han, Catal. Today 131 (2008) 477–482.
[23] S.C. Kim, W.G. Shim, Appl. Catal. B 98 (2010) 180–185.
[24] W.Z. Si, Y. Wang, S. Zhao, F.Y. Hu, J.H. Li, Environ. Sci. Technol. 50 (2016) 4572–4578.
[25] M.H. Castaño, R. Molina, S. Moreno, App. Catal. A 492 (2015) 48–59.
[26] J. Chen, X. Chen, W.J. Xu, Z. Xu, J.Z. Chen, H.P. Jia, J. Chen, Chem. Eng. J. (2017), http://dx.doi.org/10.1016/j.cej.2017.1007.1147.
[27] H. Huang, Q.G. Dai, X.Y. Wang, Appl. Catal. B 158 (2014) 96–105.
[28] C. He, Y.K. Yu, J.W. Shi, Q. Shen, J.S. Chen, H.X. Liu, Mater. Chem. Phys. 157 (2015) 87–100.
[29] X.Y. Wang, Q. Kang, D. Li, Catal. Commun. 9 (2008) 2158–2162.
[30] W. Xingyi, K. Qian, L. Dao, Appl. Catal. B 86 (2009) 166–175.
[31] M. Baldi, V.S. Escribano, J.M.G. Amores, F. Milella, G. Busca, Appl. Catal. B 17 (1998) 175–182.
[32] M.R. Morales, B.P. Barbero, L.E. Cadús, Appl. Catal. B 74 (2007) 1–10.
[33] T. Mishra, P. Mohapatra, K.M. Parida, Appl. Catal. B 79 (2008) 279–285.
[34] F.G. Durán, B.P. Barbero, L.E. Cadús, C. Rojas, M.A. Centeno, J.A. Odriozola, Appl. Catal. B 92 (2009) 194–201.
[35] F. Arena, G. Trunfio, J. Negro, B. Fazio, L. Spadaro, Chem. Mater. 19 (2007) 2269–2276.
[36] F. Arena, G. Trunfio, J. Negro, L. Spadaro, Mater. Res. Bull. 43 (2008) 539–545.
[37] Y.S. Wu, Y.X. Zhang, M. Liu, Z.C. Ma, Catal. Today 153 (2010) 170–175.
[38] J.A. Dean, Lange's Handbook of Chemistry, 16th ed., McGraw-Hill, New York, 1992, pp. 1332–1342.
[39] B.R. Strohmeier, D.M. Hercules, J. Phys. Chem. 88 (1984) 4922–4929.
[40] F. Gaillard, P. Artizzu, Y. Brullé, M. Primet, Surf. Interface Anal. 26 (1998) 367–373.
[41] T. Zhu, S.J. Zheng, Y.G. Chen, J. Luo, H.B. Guo, Y.E. Chen, J. Mater. Sci. 49 (2014) 6118–6126.
[42] D. Delimaris, T. Ioannides, Appl. Catal. B 84 (2008) 303–312.
[43] Y. Chabre, J. Pannetier, Prog. Solid State Chem. 23 (1995) 1–130.
[44] M.R. Morales, B.P. Barbero, L.E. Cadús, Fuel 87 (2008) 1177–1186.
[45] W.J. Ma, Q. Huang, Y. Xu, Y.W. Chen, S.M. Zhu, S.B. Shen, Ceram. Int. 39 (2013) 277–281.
[46] Q.G. Dai, X.Y. Wang, G.Z. Lu, Appl. Catal. B 81 (2008) 192–202.
[47] H.C. Yao, Y.F.Y. Yao, J. Catal. 86 (1984) 254–265.
[48] L. Yu, G.Q. Diao, F. Ye, M. Sun, J.L. Zhou, Y.F. Li, Y. Liu, Catal. Lett. 141 (2011) 111–119.
[49] L.F. Liotta, M. Ousmane, G. Di Carlo, G. Pantaleo, G. Deganello, G. Marcì, L. Retailleau, A. Giroir Fendler, App. Catal. A 347 (2008) 81–88.
[50] J.M. López, A.L. Gilbank, T. García, B. Solsona, S. Agouram, L. Torrente-Murciano, Appl. Catal. B 174–175 (2015) 403–412.
[51] M. Machida, M. Uto, D. Kurogi, T. Kijima, Chem. Mater. 12 (2000) 3158–3164.
[52] L. Ma, C.Y. Seo, X.Y. Chen, K. Sun, J.W. Schwank, Appl. Catal. B 222 (2018) 44–58.
[53] G.L. Zhou, X.L. He, S. Liu, H.M. Xie, M. Fu, J. Ind. Eng. Chem. 21 (2015) 932–941.
[54] G.E. Davico, V.M. Bierbaum, C.H. DePuy, G.B. Ellison, R.R. Squires, J. Am. Chem. Soc. 117 (1995) 2590–2599.
[55] C. Leiva, D. Sutton, Organometallics 17 (1998) 4568–4572.
[56] M. Szwarc, T.M. D, J. Chem. Phys. 16 (1948) 128–136.
[57] C.P. Rader, H.A. Smith, J. Am. Chem. Soc. 84 (1962) 1443–1449.
[58] H. Lynggaard, A. Andreasen, C. Stegelmann, P. Stoltze, Prog. Surf. Sci. 77 (2004) 71–137.
[59] P. Yang, Z.N. Shi, S.S. Yang, R.X. Zhou, Chem. Eng. Sci. 126 (2015) 361–369.
[60] J.A. Moulijn, A.E. van Diepen, F. Kapteijn, App. Catal. A 212 (2001) 3–16.
[61] N. Drenchev, I. Spassova, E. Ivanova, M. Khristova, K. Hadjiivanov, Appl. Catal. B 138–139 (2013) 362–372.
[62] W.X. Tang, X.F. Wu, G. Liu, S.D. Li, D.Y. Li, W.H. Li, Y.F. Chen, J. Rare Earth 33 (2015) 62–69.